Multichannel study of spin-exchange and hyperfine-induced frequency shift and line broadening in cold collisions of hydrogen atoms

B. Zygelman*
Department of Physics, University of Nevada Las Vegas, Las Vegas, Nevada 89154

A. Dalgarno†
Harvard-Smithsonian Center for Astrophysics, Cambridge, Massachusetts 02138

M. J. Jamieson‡
Department of Computing Science, University of Glasgow, Glasgow G12 8QQ, United Kingdom

P. C. Stancil§
Department of Physics and Astronomy and Center for Simulation Physics, The University of Georgia, Athens, Georgia 30602-2451
(Received 4 October 2002; published 28 April 2003)

We calculate the cross sections that characterize the frequency shift and broadening of the resonance magnetic hyperfine transition in atomic hydrogen due to collisions with hydrogen atoms in a masing cavity. We consider collision energies that correspond to the temperature range, 10 mK$<T<$1000 K, and introduce and apply a fully quantal, multichannel collision theory for the entire temperature range under consideration. Our results for the spin-exchange induced cross sections at room temperature, are in harmony with previous calculated values and experimental measurements. For the hyperfine-induced cross sections, our predicted values are in fair agreement with measurements at cryogenic temperatures with the exception of the hyperfine frequency shift at 0.5 K and 323 K for which we obtain a different sign. A study of possible resonance structures shows that they cannot be invoked to resolve the discrepancy and nor can any plausible modification of the $X^1\Sigma_g^+$ and $b^3\Sigma_u^+$ interaction potentials.

DOI: 10.1103/PhysRevA.67.042715 PACS number(s): 34.10.+x, 34.50.−s, 84.40.Ik

I. INTRODUCTION

Collisions that alter the spin angular momentum of atoms play an important role in a wide range of applications and environments, including the interstellar medium [1–3], planetary atmospheres [4–6], medical imaging [7,8], and in the operation of the hydrogen maser [9–11]. In the latter system, spin-changing collisions among hydrogen atoms in the masing cavity result in a shift [12] and broadening [13] of the observed magnetic-resonance line.

In the elastic approximation [14], hyperfine transitions occur when atoms with nearly degenerate states of different spin evolve along separate, nondegenerate molecular curves during a close encounter. Interference between the accumulated molecular phase histories [15] result in a spin-changing atomic transition. The success of the elastic approximation [5,16–22] derives from the fact that the hyperfine interaction, which lifts the degeneracy of atomic levels of different spin, is weak and for collision energies above 10 K may be neglected.

The assumption of degenerate hyperfine levels was used by Balling *et al.* [10] and Crampton [11,23] to derive expressions for the cross sections that determine the frequency shift and line broadening of the observed atomic hyperfine transition lines in a hydrogen maser. Crampton [11,23] introduced a novel technique, called spin-exchange tuning, that exploits the frequency shift and broadening due to spin-changing collisions in order to increase the stability, and enhance the performance of the hydrogen maser. The assumption of degenerate hyperfine levels is justified at room temperature but Crampton and Wang [24] pointed out the deficiencies of this approximation at extremely low temperatures. They argued that the hyperfine interaction introduces additional shifts and broadening terms that were not accounted for in the previous theories [10,11,23]. They called this the *hyperfine-induced* or HI spin-exchange effect, and suggested that these terms may limit the utility of spin-exchange tuning at low temperatures.

Verhaar *et al.* [25] analyzed the evolution equation for the spin-density matrix, assuming conditions present in a hydrogen masing cavity, that included the hyperfine interaction. They derived expressions for the HI effect frequency shift and broadening cross sections and, in a series of papers [25–27], calculated their values for a range of temperatures including the sub-Kelvin region. Using the University of British Columbia (UBC) cryogenic hydrogen maser, Hayden, Hurlimann, and Hardy [28–31] found evidence for the HI effect at a maser operation temperature of 0.5 K. An earlier study by the Harvard group of Walsworth *et al.* [32] also found evidence for an HI effect at room temperature. Though the measurements of the UBC group confirmed the reality of an HI effect, the measured shift and broadening cross sections are only in fair agreement with the calculated values of Verhaar *et al.* [25].

*Also at MIT-Harvard Center for Ultra-Cold Atoms, Cambridge, MA 02139. Electronic address: bernard@physics.unlv.edu
†Electronic address: adalgarno@cfa.harvard.edu
‡Electronic address: mjj@dcs.gla.ac.uk
§Electronic address: stancil@physast.uga.edu

The hydrogen-hydrogen complex is a fundamental atomic collision system and its theoretical analysis is a useful template for application to more complex atomic systems. The interaction potential between a pair of hydrogen atoms is known to a high degree of accuracy [33–35], and so it is significant that there exists a major discrepancy between theory and experiment for this system. The major goal of this paper is to present an independent calculation of the desired collision parameters using a theory and collision code developed in our group. We present a full theoretical treatment of the collision dynamics, and we discuss possible extensions of the present theoretical approach. Because of the continued discrepancy between theory and experiment, we give an explicit expression for the multichannel potential used in this calculation. We represent the multichannel interaction potential in terms of two parameters ϵ_0 and ϵ_1 which are the potential energy functions for the Born-Oppenheimer (BO) ground $X^1\Sigma_g^+$ and $b^3\Sigma_u^+$ states, respectively. We solve, using the full quantal multichannel formalism, for the frequency shift and broadening cross section for temperatures in the range 10 mK$<T<$1000 K, and compare our results with experiment and previous calculations. In order to assess the influence of nonadiabatic effects, not rigorously included here, we investigate the behavior and the sensitivity of the calculated cross sections to the value adopted for the reduced mass of the collision system.

In Sec. I, we develop our multichannel scattering equations using a close coupling expansion, including all spin components, for the colliding ground-state hydrogen atom pair. In Sec. II, we give a brief review of spin-exchange tuning and the HI effect [24] in the hydrogen maser. In Sec. III, we present the calculated values for the frequency shift and broadening cross sections, and compare them with those obtained in previous calculations [25] and measurements [30,32]. Atomic units are used throughout, unless otherwise stated.

II. THEORY

A. Molecular close coupling equations

We assume that the interaction of two hydrogen atoms is described by the following Hamiltonian:

$$H=H_{NR}+H_{spin},$$

$$H_{NR}=\frac{1}{2M}\sum_{i=1}^{2}\mathbf{P}_i^2+\frac{1}{2m}\sum_{i=1}^{2}\mathbf{p}_i^2+\frac{1}{|\mathbf{x}_1-\mathbf{x}_2|}+\frac{1}{|\mathbf{R}_1-\mathbf{R}_2|}-\sum_{i,j=1,2}\frac{1}{|\mathbf{R}_i-\mathbf{x}_j|}. \tag{1}$$

$\mathbf{R}_i$ and $\mathbf{P}_i$ are, respectively, the proton position and conjugate momentum vectors, $\mathbf{x}_i$ and $\mathbf{p}_i$ are the corresponding electronic operators; and all coordinates are defined with respect to a common origin in an inertial frame. M is the mass of the proton and $m=1$ is the mass of the electron. H_{spin} includes all spin and magnetic couplings amongst electrons and nuclei, but in this section, we restrict our attention to H_{NR}. In order to derive a set of configuration space scattering equations for the time-independent Schrödinger equation,

$$(H_{NR}-E)|\Psi\rangle=E|\Psi\rangle, \tag{2}$$

we project H_{NR} onto a Jacobi coordinate system. There is some arbitrariness in the choice of a Jacobi coordinate system, but the one convenient for molecular calculations is

$$\mathbf{R}_{c.m.}\equiv\frac{M\mathbf{R}_1+M\mathbf{R_2}+m\mathbf{x}_1+m\mathbf{x}_2}{2(M+m)},$$

$$\mathbf{R}\equiv\mathbf{R}_2-\mathbf{R}_1,$$

$$\mathbf{r}_i\equiv\mathbf{x}_i-\frac{(\mathbf{R}_1+\mathbf{R}_2)}{2}. \tag{3}$$

We then obtain

$$H_{NR}=H_{c.m.}+H_{KE}+H_{AD},$$

$$H_{c.m.}=-\frac{1}{4(M+m)}\boldsymbol{\nabla}_{R_{c.m.}}^2,$$

$$H_{KE}=-\frac{1}{2\mu}\boldsymbol{\nabla}_R^2,$$

$$H_{AD}=\frac{1}{2m}\sum_{i=1}^{2}\mathbf{p}_i^2+\frac{1}{4M}\left(\sum_{i=1}^{2}\mathbf{p}_i\right)^2+\frac{1}{|\mathbf{R}|}-\sum_i\frac{1}{|\mathbf{r}_i+\mathbf{R}/2|}-\sum_i\frac{1}{|\mathbf{r}_i-\mathbf{R}/2|}+\frac{1}{|\mathbf{r}_1-\mathbf{r}_2|}, \tag{4}$$

where $\mu=M/2$ is the reduced mass of the ''bare nuclei.'' We factor out the center-of-mass motion and express the eigenstate of Eq. (2) by the expansion

$$\Psi(\mathbf{R},\mathbf{r})=\sum_\gamma F_\gamma(\mathbf{R})\phi_\gamma(\mathbf{R},\mathbf{r}), \tag{5}$$

where $\phi_\gamma(\mathbf{R},\mathbf{r})$ is an eigenstate of the adiabatic Hamiltonian

$$H_{AD}\phi_\gamma(\mathbf{R},\mathbf{r})=\epsilon_\gamma(R)\phi_\gamma(\mathbf{R},\mathbf{r}). \tag{6}$$

$\epsilon_\gamma(R)$ is the Born-Oppenheimer eigenvalue [36] for state γ, and $\mathbf{r}$ is a collective label for all electronic coordinates. Index γ identifies the quantum numbers that specify a complete set of BO states, both discrete and continuous, so that

$$\sum_\gamma\phi_\gamma^*(\mathbf{R},\mathbf{r})\phi_\gamma(\mathbf{R},\mathbf{r}')=\delta^3(\mathbf{r}-\mathbf{r}'). \tag{7}$$

Inserting Eq. (5) into Eq. (2), we obtain [37],

$$-\frac{1}{2\mu}(\underline{I}\boldsymbol{\nabla}_R-i\underline{\mathbf{A}})^2\underline{F}(\mathbf{R})+\underline{V}(R)\underline{F}(\mathbf{R})=E\underline{F}(\mathbf{R}), \tag{8}$$

where the elements of the matrix potentials, $\underline{\mathbf{A}}$ and $\underline{V}$, are defined by

$$\mathbf{A}_{ab}(\mathbf{R}) = i\langle a|\boldsymbol{\nabla}_{\mathbf{R}}|b\rangle,$$

$$V_{ab}(R) = \langle a|H_{AD}|b\rangle = \delta_{ab}\epsilon_a(R), \tag{9}$$

and the bracket notation implies integration over all electronic coordinates. $\underline{F}(\mathbf{R})$ is a column vector whose entries are the channel amplitudes $\underline{F}_\gamma(\mathbf{R})$. Equation (8) is a representation, in the basis of adiabatic states, of the eigenvalue equation given in Eq. (2), and therefore, describes an infinite set of coupled equations. To obtain a working theory from this ''exact'' form, we impose the perturbed stationary states (PSS) approximation, in which, the summation index a is truncated to a finite value, usually chosen so that all open channels are included in Eq. (5) at a given collision energy. For collisions at cryogenic temperatures, we retain, in expansion (5), those adiabatic states that correlate to the ground states of the separated hydrogen atoms, i.e., the $b^3\Sigma_u^+$ and $X^1\Sigma_g^+$ BO states of the H_2 molecule. With this approximation, Eq. (8) reduces to

$$-\frac{1}{2\mu}\underline{I}\boldsymbol{\nabla}_R^2\underline{F}(\mathbf{R}) + [\underline{V}(R) + \underline{U}]\underline{F}(\mathbf{R}) = E\underline{F}(\mathbf{R}),$$

$$\underline{U}_{ab} = \frac{1}{2\mu}\sum_{k\neq(a,b)}\mathbf{A}_{ak}\cdot\mathbf{A}_{kb}, \tag{10}$$

where $\underline{F}$ is a finite dimensional column vector, and we used the fact that the nonadiabatic vector coupling matrix $\mathbf{A}$ between the $b^3\Sigma_u^+$ and $X^1\Sigma_g^+$ electronic states vanish. $\underline{U}$ is an adiabatic correction to the BO potential $\underline{V}$. In Eq. (10), the notation $\Sigma_{k\neq(a,b)}$ implies that the sum does not include any member of the set in the close coupling expansion.

In order to include the effects of nuclear spin, we generalize this procedure and introduce channel basis states that are direct products of the electronic adiabatic states, defined above, and nuclear-spin states.

The adiabatic Hamiltonian H_{AD}, and its eigenfunctions, are parametrized by the internuclear separation vector $\mathbf{R} = \{R, \theta, \phi\}$. We define Born-Oppenheimer states as those adiabatic states where $\theta = 0$ and $\phi = 0$ i.e., the nuclear vector $\mathbf{R}$ is aligned along the z axis of the laboratory frame. We label the BO states with the value of the total electronic orbital angular momentum along the z axis; the discrete quantum numbers that characterize parity, reflection, and nuclear inversion symmetries, as well as S and Σ, the total electronic spin and its component along the z axis, respectively. We identify the $b^3\Sigma_u^+$ and $X^1\Sigma_g^+$ BO states of the H_2 molecule with the ket notation $|S\Sigma\boldsymbol{\pi}\rangle$, where $\boldsymbol{\pi} = \pm 1$ are the quantum numbers that characterizes the electronic parity of the ground BO states of H_2, and $S\Sigma$ are the spin quantum numbers defined above. If we enforce the Pauli principle on these states then $\boldsymbol{\pi} = 1$ when $S = 0$, and $\boldsymbol{\pi} = -1$ when $S = 1$, and the π quantum number becomes redundant. In the discussion below, and in our tables, we will, therefore, suppress, unless otherwise stated, the electronic inversion quantum number in labeling the adiabatic electronic states. Adiabatic eigenstates are constructed by rotating the BO eigenstates into the direction $\{\theta\phi\}$; i.e., since [37]

TABLE I. Quantum numbers associated with the various basis representations. The channel index labels the states that correspond to the listed quantum numbers in each representation. The last column identifies the states that correspond to the channel index itemized under the $|F_aM_aF_bM_b\rangle$ basis, using the notation given in Fig. 1

Channel	$\lvert FMF_aF_b\rangle$	$\lvert S\Sigma IM_I\rangle$	$\lvert F_aM_aF_bM_b\rangle$	Level
1	0 0 0 0	0 0 0 0	0 0 0 0	*aa*
2	0 0 1 1	0 0 1 0	1 0 1 0	*cc*
3	1 0 0 1	1 0 0 0	0 0 1 0	*ac*
4	1 0 1 0	1 0 1 0	1 0 0 0	*ca*
5	1 0 1 1	1 −1 1 1	1 −1 1 1	*bd*
6	2 0 1 1	1 1 1 −1	1 1 1 −1	*db*
7	1 1 0 1	0 0 1 1	0 0 1 1	*ad*
8	1 1 1 0	1 1 0 0	1 1 0 0	*da*
9	1 1 1 1	1 1 1 0	1 0 1 1	*cd*
10	2 1 1 1	1 0 1 1	1 1 1 0	*dc*
11	1 −1 0 1	0 0 1−1	0 0 1 −1	*ab*
12	1 −1 1 0	1 −1 0 0	1 −1 0 0	*ba*
13	1 −1 1 1	1 −1 1 0	1 −1 1 0	*bc*
14	2 −1 1 1	1 0 1 −1	1 0 1 −1	*cb*
15	2 2 1 1	1 1 1 1	1 1 1 1	*dd*
16	2 −2 1 1	1 −1 1 −1	1 −1 1 −1	*bb*

$$H_{ad}(R\theta\phi, \mathbf{r}) = R(\theta\phi)H_{BO}(R, \mathbf{r})R(\theta\phi)^\dagger, \tag{11}$$

we require

$$\phi_a(\mathbf{R}, \mathbf{r}) = R(\theta\phi)|S\Sigma\rangle, \tag{12}$$

where

$$R(\theta\phi) = \exp(-i\phi\mathbf{L}_z)\exp(-i\theta\mathbf{L}_y)\exp(i\phi\mathbf{L}_z) \tag{13}$$

and $\mathbf{L}$ is the electronic orbital angular-momentum operator defined with respect to the molecular center.

We introduce the direct product

$$|IM_I S\Sigma\rangle \equiv |IM_I\rangle \otimes |S\Sigma\rangle, \tag{14}$$

where $|IM_I\rangle$ is an eigenstate with total nuclear angular momentum I and its projection M_I along the z axis. The adiabatic eigenstates are constructed using the prescription

$$\phi_\gamma(\mathbf{R}, \mathbf{r}) = R(\theta\phi)|IM_I S\Sigma\rangle. \tag{15}$$

Employing this basis in the close coupling expansion, Eq. (5), we obtain coupled Schrödinger equations of the form given by Eq. (8). In this picture, the scattering amplitude $F_\gamma(\mathbf{R})$ is labeled by the quantum numbers $\gamma = \{IM_I S\Sigma\}$. The quantum numbers associated with this basis are itemized in Table I. In the first column of Table I, we list the channel numbers n that range in value from 1 to 16 and identify the row of the column $\underline{F}(\mathbf{R})$. In the column headed $|IM_I S\Sigma\rangle$ in Table I, we associate a member of the set $\{IM_I S\Sigma\}$, to a particular channel. For example, channel 2, or row 2 of $\underline{F}(\mathbf{R})$, is associated with quantum numbers $I = 1$, $M_I = 0$, $S = 0$, and $\Sigma = 0$.

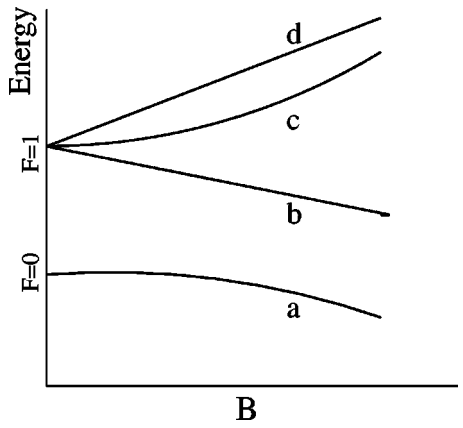

FIG. 1. Hyperfine level structure of ground-state atomic hydrogen in a magnetic field. The labels *a*, *b*, *c*, and *d* correspond to the hyperfine magnetic quantum numbers $m_F=0$, -1, 0, and 1, respectively. F is the total hyperfine quantum number.

We may also construct a close coupling expansion using basis states $|FM_FF_aF_b\rangle$, where F is the eigenvalue for the total angular momentum $\mathbf{F}=\mathbf{I}+\mathbf{S}$, and M_F is its z component. F_a and F_b are the quantum numbers corresponding to the total hyperfine operators $\mathbf{F}_a=\mathbf{S}_a+\mathbf{I}_a$ and $\mathbf{F}_b=\mathbf{S}_b+\mathbf{I}_b$ for hydrogen atom *a* and *b*, respectively. Introducing

$$\phi_\gamma(\mathbf{R},\mathbf{r})=R(\theta\phi)|FM_FF_aF_b\rangle, \tag{16}$$

into the close coupling ansatz, Eq. (5), we arrive at Eq. (8) for amplitude $\underline{F}(\mathbf{R})$ in this representation. The row numbers for $\underline{F}(\mathbf{R})$ are also denoted with the channels numbers given in Table I, but they are now associated with a new set of quantum numbers $F\,M_F\,F_a\,F_b$, itemized by the column headed $|FM_FF_aF_b\rangle$.

Finally, we introduce a third representation characterized by the kets $|F_aM_aF_bM_b\rangle$, where M_a and M_b are the z components (in the laboratory frame) of the hyperfine states of atom *a* and *b*, respectively, in the separated atom limit. The channel numbers in this representation identify the quantum numbers listed in the column of Table I headed by $|F_aM_aF_bM_b\rangle$.

In the last column of Table I, we itemize each channel with a notation commonly found in the literature. This labeling is isomorphic to the quantum number listing given in the column labeled by quantum numbers $F_aM_aF_bM_b$, and it is illustrated in Fig. 1 that shows the energy level diagrams of the $F=0$ and $F=1$ hyperfine states, for a hydrogen atom in a constant magnetic field along the z direction, in order of increasing energy. In Table I, we have grouped the channel states in terms of the total azimuthal angular momentum for the pair of atoms. The channels labeled 1–6 have total $M=0$, etc. This grouping proves to be convenient in the subsequent analysis. In each representation, we must consider a set of 16 coupled equations of the form given by Eq. (10). Since our close coupling expansion involves electronic wave functions with null orbital angular momentum along the z axis, the potential matrix $\underline{V}$ is isotropic and does not depend on the orientation angles ϕ and θ in any of the three representations. Therefore, we can further simplify Eq. (10) via a partial wave expansion. We write

$$\underline{F}(\mathbf{R})=\sum_{lm} R^{-1}\underline{F}_{lm}(R)Y_{lm}(\theta\phi), \tag{17}$$

where $\underline{F}_{lm}(R)$ is a radial column vector. Inserting Eq. (17) into Eq. (10), we obtain

$$-\frac{1}{2\mu}\left(\frac{d^2}{dR^2}-\frac{l(l+1)}{R^2}\right)\underline{F}_{lm}(R)+[\underline{V}(R)+\underline{U}(R)]\underline{F}_{lm}(R) =E\underline{F}_{lm}(R). \tag{18}$$

$\underline{F}_{lm}(R)$ is a column matrix whose γth row entry identifies the partial wave radial amplitude for channel γ. The channel, or row, index identifies the quantum numbers in the representation considered. In the discussion below, we will suppress the azimuthal quantum number label m on the radial amplitude.

The column vectors $\underline{F}_l(R)$ in each of the three representations are related, as shown below, by unitary transformations. The potential matrix $\underline{V}$ is representation dependent. In the $I\,M_I\,S\,\Sigma$ representation, $\underline{V}$ is diagonal with entries that are the BO eigenvalues. In the other two representations, $\underline{V}$ contains off-diagonal elements.

According to the previous paragraphs

$$\Psi(\mathbf{R},\mathbf{r})=\sum_{IM_IS\Sigma} F_{IM_IS\Sigma}(\mathbf{R})R(\theta\phi)|IM_IS\Sigma\rangle, \tag{19}$$

or

$$\Psi(\mathbf{R},\mathbf{r})=\sum_{F_aM_aF_bM_b} F_{F_aM_aF_bM_b}(\mathbf{R})\,R(\theta\phi)|F_aM_aF_bM_b\rangle. \tag{20}$$

Comparing Eq. (19) with Eq. (20), we find

$$F_{IM_IS\Sigma}(\mathbf{R})=\sum_{FM_F} F_{F_aM_aF_bM_b}(\mathbf{R})\langle IM_IS\Sigma|F_aM_aF_bM_b\rangle. \tag{21}$$

We express the transition amplitude $\langle IM_IS\Sigma|F_aM_aF_bM_b\rangle$ in terms of an intermediate representation,

$$\langle IM_IS\Sigma|F_aM_aF_bM_b\rangle=\sum_{FM_F}\langle IM_IS\Sigma|FM_FF_aF_a\rangle \times\langle FM_FF_aF_a|F_aM_aF_bM_b\rangle. \tag{22}$$

Now,

$$\langle IM_I S\Sigma|FM_F F_a F_a\rangle = [F,F_a,F_b,S,I]^{1/2}(-1)^{F+M_F} \times \begin{pmatrix} S & F & I \\ \Sigma & -M_F & M_I \end{pmatrix} \times \begin{Bmatrix} 1/2 & 1/2 & F_a \\ 1/2 & 1/2 & F_b \\ S & I & F \end{Bmatrix}, \quad (23)$$

and

$$\langle FM_F F_a F_b|F_a M_a F_b M_b\rangle = (-1)^{F_b-F_a-M_F}[F]^{1/2} \times \begin{pmatrix} F_a & F_b & F \\ M_a & M_b & -M \end{pmatrix}; \quad (24)$$

therefore,

$$\langle IM_I S\Sigma|F_a M_a F_b M_b\rangle = \sum_{FM_F} (-1)^{F_b-F_a+F}[F] \times \begin{pmatrix} F_a & F_b & F \\ M_a & M_b & -M \end{pmatrix} \times [F_a,F_b,S,I]^{1/2} \times \begin{pmatrix} S & F & I \\ \Sigma & -M_F & M_I \end{pmatrix} \times \begin{Bmatrix} 1/2 & 1/2 & F_a \\ 1/2 & 1/2 & F_b \\ S & I & F \end{Bmatrix}. \quad (25)$$

Using relation (21), we find that the potential matrix in the $F_a M_a F_b M_b$ representation is related to $\underline{V}(R)$ in the $IM_I S\Sigma$ representation, according to

$$V^{F_a' M_a' F_b' M_b'}_{F_a M_a F_b M_b} = \sum_{I'' M_I'' S'' \Sigma''} \langle F_a M_a F_b M_b|I'' M_I'' S'' \Sigma''\rangle \times \langle \Sigma'' S'' M_I'' I''|F_a' M_a' F_b' M_b'\rangle V^{\Sigma'' S'' M_I'' I''}_{\Sigma'' S'' M_I'' I''}$$

$$= \sum_{FM} \sum_{SI} (-1)^{F_a+F_b-F_a'-F_b'}[F,S,I] \times [F_a,F_a',F_b,F_b']^{1/2} \begin{pmatrix} F_a & F_b & F \\ M_a & M_b & -M \end{pmatrix} \times \begin{pmatrix} F_a' & F_b' & F \\ M_a' & M_b' & -M \end{pmatrix} \begin{Bmatrix} 1/2 & 1/2 & F_a \\ 1/2 & 1/2 & F_b \\ S & I & F \end{Bmatrix} \times \begin{Bmatrix} 1/2 & 1/2 & F_a' \\ 1/2 & 1/2 & F_b' \\ S & I & F \end{Bmatrix} \epsilon_S(R), \quad (26)$$

and we used the notation where the superscript label identifies the the column entry for $\underline{V}$ and the subscript the row entry. In deriving Eq. (26), we made use of the fact that the $\underline{V}$ matrix is diagonal in the $IM_I S\Sigma$ representation, and the eigenvalues $\epsilon_S(R)$ depend only on the electron spin S.

The angular coefficients appearing in Eq. (26) are evaluated and the results are summarized in Tables II–IV. In these tables, the potential matrix, for each of the three representations, is tabulated with the rows and columns designating the channel index for a particular representation. According to the channel classification outlined in Table I, the potential matrix has the following block diagonal structure:

$$\underline{V} = \begin{pmatrix} \underline{V}_1 & & & \\ & \underline{V}_2 & & \\ & & \underline{V}_3 & \\ & & & \underline{V}_4 \end{pmatrix}, \quad (27)$$

where $\underline{V}_1$ is a 6×6 matrix ranging channels 1–6, $\underline{V}_2$ is a 4×4 matrix ranging channels 7–10, $\underline{V}_3$ is a 4×4 matrix ranging channels 11–14, and $\underline{V}_4$ is a 2×2 matrix ranging channels 15–16. The block diagonal structure is invariant in each representation, but the individual submatrices V_i depend, as is shown in Tables II–IV, on the representation.

Equation (18) is the starting point for the numerical solution of the scattering amplitudes. As discussed above, this equation may be expressed in three different representations, the simplest of which is the molecular picture where the potential matrix $\underline{V}$ is diagonal. The leading contribution to the molecular potentials are the Born-Oppenheimer eigenvalues $\epsilon_S(R)$, followed by much smaller nuclear mass-dependent corrections [33,34,38]. These corrections arise from several sources, primarily the mass polarization term in Eq. (4) and the nuclear kinetic-energy correction given by the matrix $\underline{U}$ defined in Eq. (4).

There are also nonadiabatic corrections that involve nuclear momentum couplings to distant, or closed channel, electronic states. These corrections are not included in the PSS formalism since the expansion over channel states in Eq. (6) is truncated. Accurate molecular calculations must also allow for relativistic corrections [35] [We incorporate them as a correction to the eigenvalues $\epsilon_S(R)$.]

The molecular expansion described above, without inclusion of nonadiabatic couplings to distant closed channels, does not give solutions that merge, in the asymptotic region, to the wave functions that describe two noninteracting hydrogen atoms. The reduced mass μ, in the effective Schrödinger Equation (4) is that of two bare nuclei, instead of two hydrogen atoms. Also, the potentials $\underline{V}+\underline{U}$ do not give the correct, asymptotic dissociation energies. However, the introduction of an additional, adiabatic electron kinetic-energy correction [33,38] can be included to give more accurate dissociation energies. At first sight these corrections appear to be small, however, it is known [39] that the failure of the PSS approximation to allow an accurate asymptotic description may lead to its break down at large collision energies.

TABLE II. Elements of the potential matrix $\underline{V}_1$ for each of the three representations discussed in the text. The representations are labeled with the corresponding quantum numbers $\{IM_I S\Sigma\}$, $\{FM_F F_a F_b\}$, and $\{F_a M_a F_b M_b\}$. The rows and columns correspond to channels 1–6 in Table I.

$IM_I S\Sigma$					
ϵ_0	0	0	0	0	0
	ϵ_0	0	0	0	0
		ϵ_1	0	0	0
			ϵ_1	0	0
				ϵ_1	0
					ϵ_1
$FM_F F_a F_b$					
$\frac{(\epsilon_0+3\epsilon_1)}{4}$	$\frac{\sqrt{3}(\epsilon_0-\epsilon_1)}{4}$	0	0	0	0
	$\frac{(3\epsilon_0+\epsilon_1)}{4}$	0	0	0	0
		$\frac{(\epsilon_0+3\epsilon_1)}{4}$	$\frac{(\epsilon_1-\epsilon_0)}{4}$	$\frac{(\epsilon_0-\epsilon_1)}{2\sqrt{2}}$	0
			$\frac{(\epsilon_0+3\epsilon_1)}{4}$	$\frac{(\epsilon_1-\epsilon_0)}{2\sqrt{2}}$	0
				$\frac{(\epsilon_0+\epsilon_1)}{2}$	0
					ϵ_1
$F_a M_b F_b M_b$					
$\frac{(\epsilon_0+3\epsilon_1)}{4}$	$\frac{(\epsilon_1-\epsilon_0)}{4}$	0	0	$\frac{(\epsilon_0-\epsilon_1)}{4}$	$\frac{(\epsilon_0-\epsilon_1)}{4}$
	$\frac{(\epsilon_0+3\epsilon_1)}{4}$	0	0	$\frac{(\epsilon_1-\epsilon_0)}{4}$	$\frac{(\epsilon_1-\epsilon_0)}{4}$
		$\frac{(\epsilon_0+3\epsilon_1)}{4}$	$\frac{(\epsilon_1-\epsilon_0)}{4}$	$\frac{(\epsilon_1-\epsilon_0)}{4}$	$\frac{(\epsilon_0-\epsilon_1)}{4}$
			$\frac{(\epsilon_0+3\epsilon_1)}{4}$	$\frac{(\epsilon_0-\epsilon_1)}{4}$	$\frac{(\epsilon_1-\epsilon_0)}{4}$
				$\frac{(\epsilon_0+\epsilon_1)}{2}$	0
					$\frac{(\epsilon_0+\epsilon_1)}{2}$

There is evidence [19,25] that the replacement of reduced mass μ with μ_H, the reduced mass for two hydrogen atoms, significantly affects the calculated values for the spin-exchange cross sections. The results of our calculations show that there is a large variation in the calculated values for the frequency shift and broadening cross sections with the adopted values for the reduced mass for the system.

In Ref. [25], it was argued that μ_H, rather than μ, be used in the effective radial equation for the atom pair, since the former may account for nonadiabatic effects not included in the scattering formalism. Though this assumption is based on nonrigorous arguments, we calculate the cross sections for both values of reduced mass in order to explore, and assess, the sensitivity of these cross sections to nonadiabatic effects. In the Appendix, we provide a rigorous molecular framework in which the atom reduced mass μ_H is accounted for from first principles. We use state-of-the-art BO ground-state potentials that are discussed in more detail in Ref. [47].

B. Hyperfine interactions

H_{spin} describes the coupling of the electronic and nuclear-spin angular momenta. The largest contribution to H_{spin} arises from the interaction between the magnetic fields generated by the proton and the spin of the electron. For the ground-state hydrogen atom, the leading interaction is given by the Fermi contact term,

$$A_F \mathbf{I}\cdot\mathbf{S}, \tag{28}$$

where $A_F = 0.047\,38\ \mathrm{cm}^{-1}$, $\mathbf{I}$ is the spin of the nucleus, and $\mathbf{S}$ the spin of the electron. In previous calculations [25,27], the atom-atom hyperfine interaction was taken to have the form

$$H_{spin} = A_F[\mathbf{I}_1\cdot\mathbf{S}_1 + \mathbf{I}_2\cdot\mathbf{S}_2]. \tag{29}$$

TABLE III. Elements of the potential matrix $\underline{V}_2$ for each of the three representations discussed in the text. The representations are labeled with the corresponding quantum numbers $\{IM_I S\Sigma\}$, $\{FM_F F_a F_b\}$, and $\{F_a M_a F_b M_b\}$. The rows and columns correspond to channels 7–10 in Table I.

$IM_I S\Sigma$			
ϵ_0	0	0	0
	ϵ_1	0	0
		ϵ_1	0
			ϵ_1
$FM_F F_a F_b$			
$\frac{(\epsilon_0+3\epsilon_1)}{4}$	$\frac{(\epsilon_1-\epsilon_0)}{4}$	$\frac{(\epsilon_0-\epsilon_1)}{2\sqrt{2}}$	0
	$\frac{(\epsilon_0+3\epsilon_1)}{4}$	$\frac{(\epsilon_1-\epsilon_0)}{2\sqrt{2}}$	0
		$\frac{(\epsilon_0+\epsilon_1)}{2}$	0
			ϵ_1
$F_a M_a F_b M_b$			
$\frac{(\epsilon_0+3\epsilon_1)}{4}$	$\frac{(\epsilon_1-\epsilon_0)}{4}$	$\frac{(\epsilon_1-\epsilon_0)}{4}$	$\frac{(\epsilon_0-\epsilon_1)}{4}$
	$\frac{(\epsilon_0+3\epsilon_1)}{4}$	$\frac{(\epsilon_0-\epsilon_1)}{4}$	$\frac{(\epsilon_1-\epsilon_0)}{4}$
		$\frac{(\epsilon_0+3\epsilon_1)}{4}$	$\frac{(\epsilon_1-\epsilon_0)}{4}$
			$\frac{(\epsilon_0+3\epsilon_1)}{4}$

TABLE IV. Elements of the potential matrix $\underline{V}_3$ for each of the three representations discussed in the text. The representations are labeled with the corresponding quantum numbers $\{IM_I S\Sigma\}$, $\{FM_F F_a F_b\}$, and $\{F_a M_a F_b M_b\}$. The rows and columns correspond to channels 11–14 in Table I.

$IM_I S\Sigma$			
ϵ_0	0	0	0
	ϵ_1	0	0
		ϵ_1	0
			ϵ_1
$FF_M F_a F_b$			
$\frac{(\epsilon_0+3\epsilon_1)}{4}$	$\frac{(\epsilon_1-\epsilon_0)}{4}$	$\frac{(\epsilon_0-\epsilon_1)}{2\sqrt{2}}$	0
	$\frac{(\epsilon_0+3\epsilon_1)}{4}$	$\frac{(\epsilon_1-\epsilon_0)}{2\sqrt{2}}$	0
		$\frac{(\epsilon_0+\epsilon_1)}{2}$	0
			ϵ_1
$F_a M_a F_b M_b$			
$\frac{(\epsilon_0+3\epsilon_1)}{4}$	$\frac{(\epsilon_1-\epsilon_0)}{4}$	$\frac{(\epsilon_1-\epsilon_0)}{4}$	$\frac{(\epsilon_0-\epsilon_1)}{4}$
	$\frac{(\epsilon_0+3\epsilon_1)}{4}$	$\frac{(\epsilon_0-\epsilon_1)}{4}$	$\frac{(\epsilon_1-\epsilon_0)}{4}$
		$\frac{(\epsilon_0+3\epsilon_1)}{4}$	$\frac{(\epsilon_1-\epsilon_0)}{4}$
			$\frac{(\epsilon_0+3\epsilon_1)}{4}$

This Hamiltonian reproduces the correct asymptotic hyperfine splitting for each atom since in the $|F_a M_a F_b M_b\rangle$ and $|FMF_a F_b\rangle$ representations, the hyperfine interaction potential matrices are given by

$$V^{F_a' M_a' F_b' M_b'}_{F_a M_a F_b M_b} = \delta_{F_a' F_a}\delta_{F_b' F_b}\delta_{M_a' M_a}\delta_{M_b' M_b}\frac{A_F}{2}[F_a(F_a+1) + F_b(F_b+1)-3] \tag{30}$$

and

$$V^{F' M_{F'} F_a' F_b'}_{F M_F F_a F_b} = \delta_{F' F}\delta_{M_{F'} M_F}\delta_{F_a' F_a}\delta_{F_b' F_b}\frac{A_F}{2}[F_a(F_a+1) + F_b(F_b+1)-3], \tag{31}$$

respectively. Though expression (29) is invariant under atom interchange, it is not symmetric under the interchange of electrons, as well as the interchange of protons, and is therefore, formally incomplete. Indeed, the phenomenological, molecular hyperfine contact interaction has the form [41]

$$H_{eff} = aI_z + b\mathbf{I}\cdot\mathbf{S} + cI_z S_z, \tag{32}$$

where $\mathbf{S}=\mathbf{S}_1+\mathbf{S}_2$ is the total electronic spin, $\mathbf{I}=\mathbf{I}_1+\mathbf{I}_2$ is the total nuclear spin, and a, b, and c are constants. The subscript z denotes the vector component along the internuclear axis. Expression (32) predicts the correct hyperfine structure for the bound hydrogen molecule, and differs from that obtained using Eq. (29) by terms that are quadratic in the Fermi constant A_F. These small differences do not affect the scattering solution in the molecular region since, in that region, the differences in the singlet and triplet molecular potentials are much larger than the hyperfine interaction. However, in regions where the energy defect between the singlet and triplet molecular potentials has the same magnitude as the hyperfine interaction, the scattering solutions could be sensitive to details in the hyperfine Hamiltonian.

We propose the following atom-atom Fermi contact interaction:

$$H_{hf} = A[\delta^3(\mathbf{r}_1+\mathbf{R}/2)\mathbf{I}_1\cdot\mathbf{S}_1 + \delta^3(\mathbf{r}_1-\mathbf{R}/2)\mathbf{I}_2\cdot\mathbf{S}_1 + \delta^3(\mathbf{r}_2-\mathbf{R}/2)\mathbf{I}_1\cdot\mathbf{S}_2 + \delta^3(\mathbf{r}_2+\mathbf{R}/2)\mathbf{I}_2\cdot\mathbf{S}_2], \tag{33}$$

where $\mathbf{r}_1$ and $\mathbf{r}_2$ are electronic coordinates and A is a constant. Expression (33) satisfies the required symmetry property, under identical particle interchange, and has the correct separated atom limit. However, its representation with respect to the Born-Oppenheimer ground-state wave functions introduces molecular screening and exchange effects that are not evident in expressions (30) and (31) for the effective hyperfine interaction. We hope to explore the sensitivity of the cross sections on the choice for the effective spin Hamil-

tonian in future studies. In addition to the contact interaction, we must also include the long-range magnetic Breit [40], or dipolar, interactions between atoms. These terms are expected to provide a small correction to the elastic cross sections [27], and a full accounting of these effects will be deferred to future studies.

C. Asymptotic boundary conditions

In the $F_aM_aF_bM_b$ representation, the hyperfine interaction given in Eq. (30) is a constant diagonal matrix, and in the asymptotic region, it represents the energy shift induced by the Fermi contact interaction in each atom. We numerically solve coupled equations (18), including the hyperfine potential given in Eq. (30), for the radial amplitudes. There exist $n=16$ independent solutions and we reexpress the partial wave amplitude $\underline{F}_l(R)$ as a square matrix [42]. Each column of the $n\times n$ matrix represents a linearly independent solution of Eq. (18), and the n vectors are chosen in order that $\underline{F}_l(R)$ satisfies the asymptotic boundary condition

$$\lim_{R\to\infty}\underline{F}_l(R)=\underline{J}_l(kR)-\underline{N}_l(kR)\underline{K}_l, \tag{34}$$

where

$$\underline{J}_l(kR)_{ij}=\delta_{ij}j_l(k_iR)/\sqrt{k_i},$$

$$\underline{N}_l(kR)_{ij}=\delta_{ij}n_l(k_iR)/\sqrt{k_i}. \tag{35}$$

Here δ_{ij} is the Kronecker delta function, $j_l(kR)$ and $n_l(kR)$ are, respectively, the regular and irregular Bessel-Ricatti functions; and

$$k_i=\sqrt{2\mu[E-V_i(\infty)]} \tag{36}$$

is the wave number for the relative kinetic energy of the system in channel *i*. Relation (35) is used to calculate the *K* matrix $\underline{K}$, from which, the *S* matrix is obtained,

$$\underline{S}=(\underline{I}+i\underline{K})^{-1}(\underline{I}-i\underline{K}). \tag{37}$$

For channels that are closed, we use the method of Johnson [43] to construct the *S* matrix. Once the *S* matrix is calculated, we can describe the various cross sections that characterize the collision induced frequency shift and line broadening. We carry out the calculations using the $F_aM_aF_bM_b$ basis since that is the representation in which the labeling of atomic states, shown in Fig. 1, is made and the cross sections [25] are defined. However, since each representation is related by a unitary transformation so is the *S* matrix. If the $\{IMS\Sigma\}$ basis is used, including the hyperfine interaction, then the asymptotic solution no longer has the form given by Eq. (34) since the hyperfine interaction contains asymptotic off-diagonal terms in this representation. If the hyperfine interaction is not included, the multichannel equations in the $\{IMS\Sigma\}$ picture reduce to diagonal form and the solutions are simply expressed in terms of the elastic phase shifts for the triplet and singlet ground state potentials. Transforming the diagonal *S* matrix into the $\{F_aM_aF_bM_b\}$ representation, gives the spin-changing cross section in terms of the elastic scattering phase shifts, this is the essence of the elastic approximation [14].

III. SPIN-EXCHANGE TUNING IN THE HYDROGEN MASER

A. Introduction

The high stability of the hydrogen maser operating at room temperature is due, in part, to a method called *spin-exchange tuning*. Developed by Crampton [11,12,23] spin-exchange tuning exploits a relationship between the operating frequency of the maser and the parameters that define the collision properties of the atoms at the microscopic level. According to the classical theory of Crampton, the frequency offset $\delta\omega$ due to the combined effects of collisions and cavity detuning is given by

$$\delta\omega=[\Delta+\beta\lambda_0(1+\Delta^2)]\Gamma, \tag{38}$$

where $\delta\omega$ is the difference between the cavity operating frequency ω, and the density independent atomic transition frequency ω_0. Δ is the cavity detuning

$$\Delta=Q\left(\frac{\omega_c}{\omega}-\frac{\omega}{\omega_c}\right), \tag{39}$$

where Q is the quality factor of the cavity and ω_c is the resonant frequency for the cavity. Γ is the full atomic linewidth and λ_0 is a frequency shift cross section that is derived from spin-exchange collision theory. β is a parameter that is proportional to the thermally averaged velocities of the constituent atoms, as well as other constants that characterize the physical properties of the maser. Atomic collisions shift the resonance frequency and fluctuations in the density of atoms in the maser could, presumably, limit the stability of the maser. Spin-exchange tuning exploits relationship (38), so that by a judicious choice for the cavity pulling, $\Delta=\Delta'\equiv-\beta\lambda_0$ and if Δ' is small, one can tune to a near null value for $\delta\omega$. When this equality is satisfied, the maser is said to be spin-exchange tuned and the operation frequency of the maser is independent of fluctuations in the hydrogen gas density. At room temperature, the measured [12] value for $\lambda_0=4.1\pm0.1\times10^{-16}$ cm^2 is in good agreement with the theoretical calculations by Allison [13], and Berlinsky and Shizgal [19].

In the late 1970's, Crampton, Phillips, and Kleppner [45] suggested that a hydrogen maser operating at cryogenic temperatures could show improved frequency stability, of two to three orders of magnitude, from that of room temperature masers. However, at low temperatures the assumptions that went into the derivation of Eq. (38), and is the basis for spin-exchange tuning, are no longer valid. At cryogenic temperatures, the hyperfine structure of the hydrogen atoms must be accounted for in the collision dynamics. The hyperfine interaction translates into a shift of about 0.07 K and neglecting it at room temperature is justified. The latter approximation is sometimes called the degenerate internal state (DIS) approximation or the elastic approximation [14]. Its adoption

greatly simplifies the collision dynamics and leads to relation (38). Crampton and Wang [24] considered the effect of hyperfine interactions, in the context of a semiclassical analysis, and they generalized relation (38) to

$$\delta\omega=[\Delta+\beta\lambda_0(1+\Delta^2)]\Gamma-\Omega\Gamma_c, \tag{40}$$

where Γ_c is a density-dependent linewidth and Ω is a dimensionless atomic collision parameter that is null in the DIS approximation. If Δ is small and if a cavity detuning $\Delta''\equiv-(\beta\lambda_0-\Omega)$ is chosen, the density-dependent linewidth in the expression for $\delta\omega$ is null. However, there still exists a shift $\delta\omega=-\Omega(\Gamma-\Gamma_c)$, and its presence limits the utility of spin-exchange tuning in a cryogenic hydrogen maser (CHM). The term proportional to Ω in Eq. (40) has been dubbed the HI effect by Crampton and, a fully quantum mechanical theory for the HI effect was proposed [25]. This theory, which we call the VKSLC theory [32], can be summarized by an equation that has the form (40), except that the parameter Ω is expressed as a complicated function of two additional frequency shift cross sections λ_1 and λ_2, and line broadening cross sections σ_0, σ_1, and σ_2, as well as the populations of the hyperfine levels of the colliding atomic pair.

B. Experimental evidence for the HI effect

Evidence for a small HI effect at room temperature was suggested in experiments by Crampton and Wang in the 1970s. Measurements, carried out in the 1990s, by the University of British Columbia Cryogenic Hydrogen Maser (UBC-CHM) group confirmed the reality of a significant effect at cryogenic temperatures [28–31]. The UBC group of Hardy, Hayden, and Hurlimann used the UBC-CHM at 0.5 K to measure Ω and λ_0. They obtained the value $\lambda_0=-21.7(2.8)\times10^{-16}$ cm^2 and for the HI effect parameter, $\Omega=-0.057^{+0.009}_{-0.021}$. Additional evidence for the HI effect was seen in experiments, using the Center for Astrophysics Hydrogen Maser (CfA-HM), by Walsworth and co-workers [32]. The CfA-HM experiments measured the $\Omega_{on}-\Omega_{off}$ parameter, a quantity that is related to Ω, and it was found to have the value $\Omega_{on}-\Omega_{off}=5.38(1.06)\times10^{-4}$ at 323 K.

C. Theory of the HI effect

The quantum mechanical basis for the HI effect was outlined within the VKSLC theory [25] that we summarize below. In the VKSLC theory, the following cross sections

$$i\lambda_0-\sigma_0\equiv\sigma^{ac}_{c\to c}-\sigma^{ac}_{a\to a},$$

$$i\lambda_1-\sigma_1\equiv\sigma^{ac}_{c\to c}+\sigma^{ac}_{a\to a}-\sigma^{ac}_{d\to d},$$

$$i\lambda_2-\sigma_2\equiv\sigma^{ac}_{d\to d}, \tag{41}$$

where

$$\sigma^{ac}_{\nu\to\nu}\equiv\frac{\pi}{k^2}\sum_l(2l+1)[S_{\{a\nu\},\{a\nu\}}(l,E)S^*_{\{c\nu\},\{c\nu\}}(l,E)-1], \tag{42}$$

are defined. The λ_0, λ_1, and λ_2 cross sections determine the frequency shift, whereas σ_0, σ_1, and σ_2 characterize the line broadening.

The labels a,c, and d are shown in Fig. 1, S is the S matrix and $\{\ \}$ is a symmetrization symbol defined, so that

$$S_{\{ac\},\{ac\}}(l,E)=\frac{1}{2}[S_{ac,ac}(l,E)\mp S_{ac,ca}(l,E)\mp S_{ca,ac}(l,E)+S_{ca,ca}(l,E)], \tag{43}$$

etc., and where $\mp$ refers to $l=$ odd and $l=$ even, respectively, E is the collision energy and k the wave number for that energy.

The S matrix is obtained by solving the set of multichannel scattering equations described in the preceding section. If we impose the elastic, or DIS, approximation, i.e., we ignore the energy defect of the hyperfine levels, considerable simplification in the expression for the S matrix follows. Indeed, in that approximation, the S matrix can be expressed in terms of elastic scattering phase shifts for the singlet $\epsilon_0(R)$, and triplet $\epsilon_1(R)$ molecular potential curves for the ground states of the separating hydrogen atoms. If we label the elastic singlet $\delta_s(l)$ and triplet $\delta_t(l)$ phase shifts, where l is the orbital angular momentum for the colliding pair, the shift and broadening cross sections reduce to the following simpler expressions:

$$\lambda_0=\frac{\pi}{2k^2}\sum_{even\ l}(2l+1)\sin(2\delta_t(l)-2\delta_s(l)),$$

$$\sigma_1=\frac{\pi}{k^2}\sum_l(-1)^l(2l+1)\sin^2(\delta_t(l)-\delta_s(l)),$$

$$\sigma_2=\frac{\pi}{k^2}\sum_{odd\ l}(2l+1)\sin^2(\delta_t(l)-\delta_s(l)),$$

$$\lambda_1=\lambda_2=\sigma_0=0. \tag{44}$$

The Ω parameter is defined in terms of these cross sections and is given by [25]

$$\Omega=-\frac{\overline{\lambda_1}(\rho_{cc}+\rho_{aa})+\overline{\lambda_2}}{\overline{\sigma_1}(\rho_{cc}+\rho_{aa})+\overline{\sigma_2}}, \tag{45}$$

where the overbar implies an averaging over a thermal velocity distribution of the cross sections. ρ_{aa} and ρ_{cc} are the diagonal elements of the hydrogen atom pair density matrix and correspond to the atom populations in the a and c hyperfine levels.

IV. RESULTS

We present the results of our calculation for the frequency shift and broadening cross sections in the figures shown below. In Figs. 2(a)–2(f), we plot the cross sections as a function of collision energy expressed in units of kT where T is the temperature in kelvins. In Figs. 2(a)–2(c), we compare the results of the multichannel calculations with those ob-

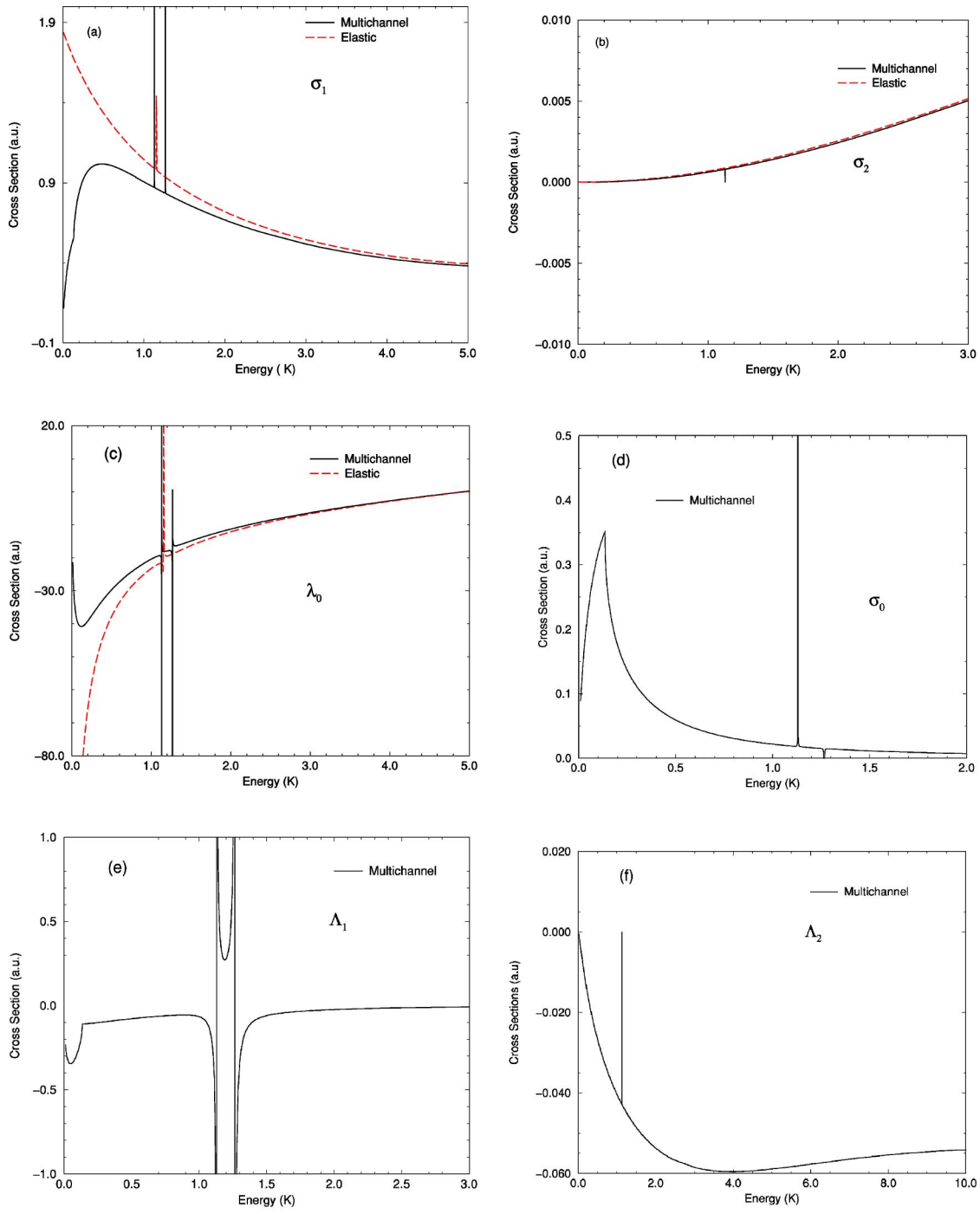

FIG. 2. Calculated values for the frequency shift and broadening cross sections. The collision energy is expressed in terms of kT where T is the temperature in kelvins. (a) σ_1, (b) σ_2, (c) λ_0, (d) σ_0, (e) λ_1, and (f) λ_2.

tained using the elastic, or DIS, approximation. The latter approximation gives accurate λ_0, σ_1, and σ_2 cross sections for temperatures $T > 3$ K. The HI effect cross sections, σ_0, λ_1, and λ_2 are shown in Figs. 2(d)–2(f). In the elastic approximation, they are identically equal to zero. The results in Fig. 2 were calculated using the atomic bare reduced mass μ, and in Figs. 3(a)–3(f), we compare them with the ones obtained using the atomic reduced masses. The calculated cross sections are extremely sensitive to the small change in the value of reduced mass. The sharp peaks are due to a shape resonance in the $J=4$ partial wave which vanishes when $\mu = 0.503\,638$ amu is replaced by $\mu_H = 0.503\,913$ amu. The double resonance peak structures, apparent in the figures, are due to hyperfine energy splittings that shift the entrance channel collision energy and, therefore, the location of the $J=4$ resonance.

In Figs. 4(a)–4(c), we plot the non-HI cross sections, λ_0, σ_1, and σ_2, for collision energies ranging up to 1000 K.

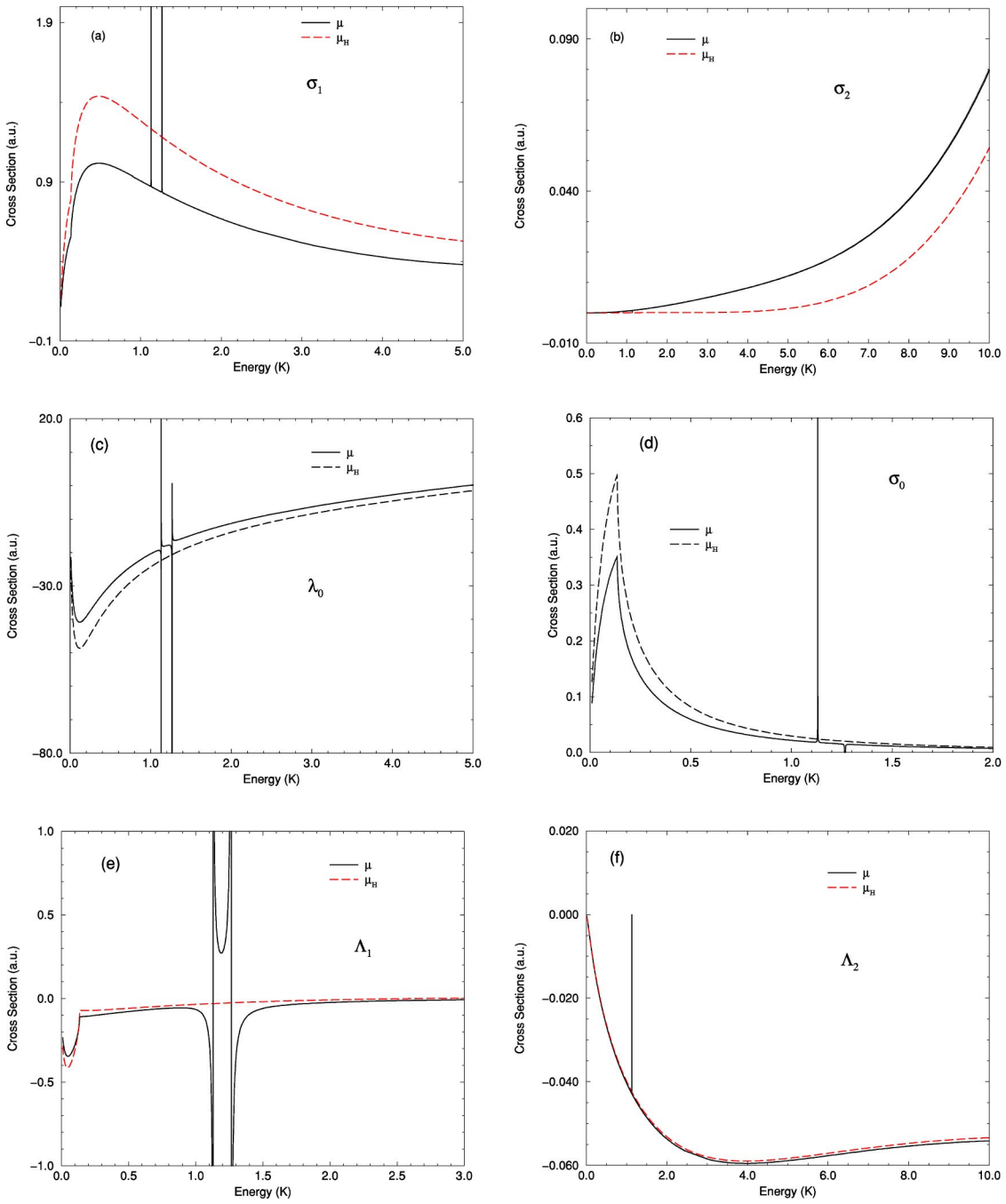

FIG. 3. Comparison of cross sections obtained using the values μ and μ_H for the reduced mass of the collision system. (a) σ_1, (b) σ_2, (c) λ_0, (d) σ_0, (e) λ_1, and (f) λ_2.

In Fig. 4(c), we also plot the measured value, at $T=308$ K, for λ_0 (note: $\lambda_0=-\lambda^+/4$, where λ^+ is the notation used in Refs. [12,17]), and find excellent agreement with our calculated value. The crosses in that figure are the thermal averaged cross section values of Allison [17]. The calculated σ_2 cross section, shown in Fig. 4(b), is in excellent agreement with the experimental measurement at room temperature. In Figs. 5(a) and 5(b), we present the results for the HI effect cross sections λ_1, λ_2, and σ_0, in the energy range up to 1000 K. In Fig. 5(b) we plot the λ_1 cross sections and compare them to an experimental measurement, at $T=323$ K, by Walsworth *et al.* [32]. They are only fair agreement between the experimental and theoretical values. However, our results are in good agreement, in this temperature region, with the theoretical calculations of Koelman *et al.* [26]

In Tables VI and VII, we tabulate the thermal averaged cross sections [25]

$$\langle\sigma\rangle\equiv\frac{\langle v\,\sigma\rangle}{\langle v\rangle}, \tag{46}$$

where σ is a cross section and the bracket notation refers to

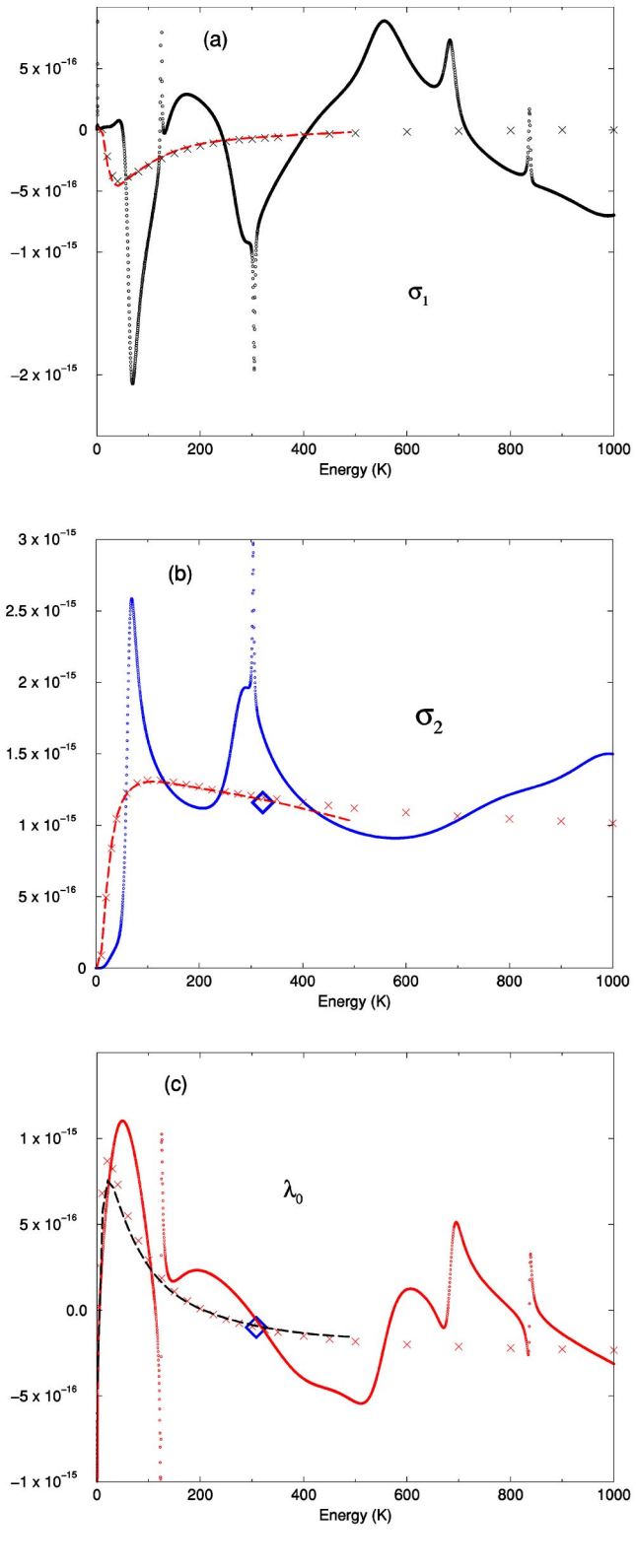

FIG. 4. Calculated values for the non-HI frequency shift and broadening cross sections in the collision energy range 1 K$\approx<T<$1000 K. The dashed lines represent the thermal average of the cross sections and the crosses denote the calculated thermal averages given by Allison [13]. (a) σ_1 and (b) σ_2, the diamond represents the value quoted in Ref. [32] for the measurements reported in Ref. [46]; (c) λ_0, the diamond represents the measurement of Crampton *et al.* [12].

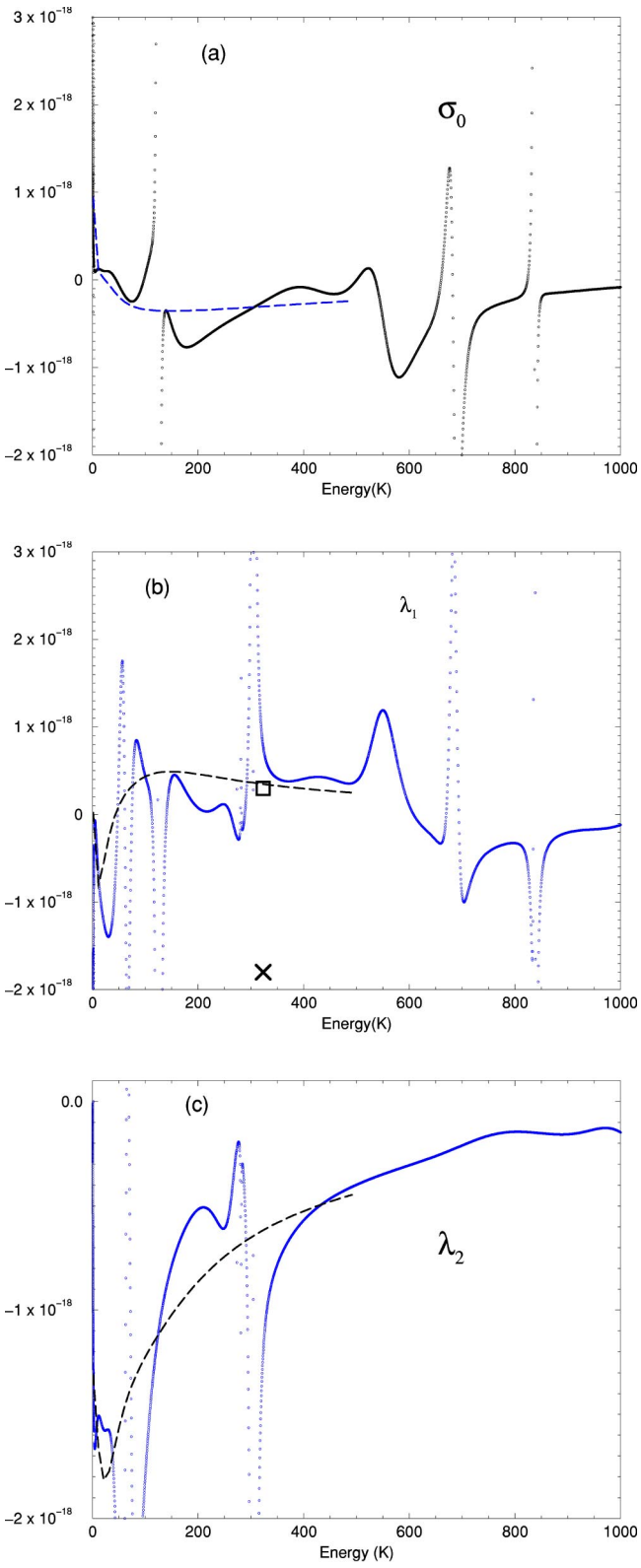

FIG. 5. Calculated values for the HI frequency shift and broadening cross sections in the collision energy range 1 K$\approx<T<$1000 K. The dashed lines represent the thermal average of the cross sections. (a) σ_0, (b) λ_1, the cross is the measured value at 323 K [32] and the box is the thermal averaged cross section given in Ref. [25]. (c) λ_2.

TABLE V. Elements of the potential matrix $\underline{V}_4$ for each of the three representations discussed in the text. The representations are labeled with the corresponding quantum numbers $\{IM_I S\Sigma\}$, $\{FM_F F_a F_b\}$, and $\{F_a M_a F_b M_b\}$. The rows and columns correspond to channels 15–16 in Table I.

$IM_I S\Sigma$	
ϵ_1	0
	ϵ_1
$FM_F F_a F_b$	
ϵ_1	0
	ϵ_1
$F_a M_a F_b M_b$	
ϵ_1	0
	ϵ_1

averaging over a Boltzmann distribution of collision energies at temperature T. In Table VI, we compare cross sections, for $T=0.5$ K, calculated using the two different values μ and μ_H for the reduced mass. We also compare the cross sections obtained using the elastic approximation with those calculated using the multichannel method. With the exception of the σ_2 cross section, the values for the thermal averaged cross sections given here are within 50% of the values (for reduced mass μ_H) reported in Ref. [25]. Presumably, the discrepancy between the two sets of calculated cross sections are due to differences in the adopted potential energy functions for the $X^+\Sigma_g^+$ and $b^3\Sigma_u^+$ electronic states. It is noteworthy that the signs of the calculated values for the HI effect cross sections λ_1 and λ_2 given here and those presented in Ref. [25] are the same, though their absolute values are somewhat different.

In Table VII, we compare the results of our calculation for the HI effect frequency shift cross section $\frac{1}{2}\lambda_1+\lambda_2$, with the measured values at 0.5 K. The calculated and measured values have different signs. Our calculated value for λ_0 is about 40% of the measured value, as is our calculated value for the broadening cross section $\frac{1}{2}\sigma_1+\sigma_2$. The λ_0, σ_1, and σ_2, cross sections obtained in the elastic approximation give somewhat better agreement with experiment. We also find that using μ_H appears to give cross sections that are closer to the measured values. Walsworth *et al.* [32] measured the dimensionless $\Omega_{on}-\Omega_{off}$ parameter, at $T=323$ K, to have the value $5.38(1.06)\times10^{-4}$. According to Ref. [32], this parameter can be approximated by $\Omega_{on}-\Omega_{off}\approx-\bar{\lambda}_1/2\bar{\sigma}_2$ for the conditions present in their masing cavity. Using the calculated values for the thermal averaged cross sections, $\bar{\lambda}_1=3.30\times10^{-19}$ cm^2 and $\bar{\sigma}_2=1.14\times10^{-15}$ cm^2, we obtain, $\Omega_{on}-\Omega_{off}=-1.45\times10^{-4}$. The calculated value has a different sign than the measured value, and it is about five standard deviations from the experimental mean value. It is in good agreement with the theoretical value -1.12×10^{-4}, quoted in Ref. [32].

V. SUMMARY AND DISCUSSION

We have calculated the cross sections that characterize the frequency shift and broadening of the resonance magnetic hyperfine transition in atomic hydrogen due to collisions with hydrogen atoms for collision energies that correspond to the temperature range, 10 mK$<T<$1000 K. We employed a fully quantal, multichannel collision theory and code for the entire temperature range under consideration. Our results for the non-HI effect cross sections are in harmony with previous calculated values [13,19,26] and experimental measurements [12,46]. However, for the predicted [25] HI effect cross sections, we find only fair agreement with the results of measurements at both room [32] and cryogenic [30] temperatures. Our predictions are consistent with the results of previous calculations reported in Refs. [25,27].

There are several possible reasons for the continued discrepancy between theory and experiment. Assuming that the VSKLC theory of the HI effect in the hydrogen maser is correct, we focus here on the deficiencies and proposed improvements in the theoretical description of the collision dynamics. In this study, we did not incorporate a rigorous treatment of nonadiabatic effects, but we did explore the dependence of the calculated cross sections on the choice for the adopted reduced mass of the system. It has been argued [19,25] that, in lieu of a rigorous treatment, the replacement of the bare nuclear reduced mass with that of the atom-atom reduced mass, provides a measure of nonadiabatic effects. Figure 3 and Table VI indicate that a variation in the value of reduced mass accounts for an order 20% variation in the cross sections. Though this effect is considerable, it does not explain the larger discrepancies between theory and experiment. It is possible, since the value in reduced mass determines the location and width of the $J=4$ shape resonance, that such an effect may account for part of these discrepancies. However, our calculations indicate that the resonance

TABLE VI. Thermal averaged cross sections at $T=0.5$ K. All cross sections are given in units of cm^2.

	μ		μ_H		
	Multichannel	Elastic	Multichannel	Elastic	Ref. [25]
λ_0	-6.54×10^{-16}	-8.80×10^{-16}	-7.81×10^{-16}	-1.06×10^{-15}	-1.19×10^{-15}
σ_1	2.46×10^{-17}	3.16×10^{-17}	3.42×10^{-17}	4.47×10^{-17}	5.24×10^{-17}
σ_2	2.48×10^{-20}	2.65×10^{-20}	1.52×10^{-21}	1.80×10^{-21}	7.48×10^{-20}
σ_0	1.78×10^{-18}	0.0	2.04×10^{-18}	0.0	4.1×10^{-18}
λ_1	-5.90×10^{-19}	0.0	-1.31×10^{-18}	0.0	-1.8×10^{-18}
λ_2	-1.00×10^{-18}	0.0	-9.89×10^{-19}	0.0	-1.2×10^{-18}

TABLE VII. Comparison of results from multichannel calculations with the measured cross sections at $T=0.5$ K.

	μ	μ_H	Ref. [27]	Ref. [30]
λ_0	-6.54×10^{-16}	-7.81×10^{-16}	-1.19×10^{-15}	$-2.17\pm0.28\times10^{-15}$
$\frac{1}{2}\lambda_1+\lambda_2$	-1.30×10^{-18}	-1.64×10^{-18}	-2.04×10^{-18}	2.2×10^{-18}
$\frac{1}{2}\sigma_1+\sigma_2$	1.23×10^{-17}	1.71×10^{-17}	2.63×10^{-17}	3.8×10^{-17}

shown in Figs. 3 and 4 does not provide a significant contribution to the thermal averaged cross sections. Measurements at several maser operation temperatures would provide some guidance on this question. Walsworth *et al.* [32] found evidence for an HI effect at room temperature. Figure 5(b) compares the measured value for $\overline{\lambda_1}$ [32] at $T=323$ K, with the results obtained in our calculations. Numerous resonance structures are apparent in that figure. In the calculations, we used an energy grid that covers the entire region with a spacing that is less than 0.3 K and so it is unlikely that a resonance of width smaller than this grid spacing could provide a significant contribution to the thermal averaged value $\overline{\lambda_1}$. Kokkelman and Verhaar [27] argued that there exists no parameterization for the short-range phase shifts that accounts for all discrepancies with the measured cross sections at $T=0.5$ K, a conclusion with which we agree. Nevertheless, it would be of interest to explain the influence of nonadiabatic effects at larger internuclear separations [47] and to consider further the influence of a formally exact theory of the hyperfine interaction.

ACKNOWLEDGMENTS

B.Z. was supported, as a Visiting Scientist, by an NSF grant to the MIT-Harvard Center for Ultracold Atoms (CUA) and the Institute for Theoretical Atomic and Molecular and Physics. A.D. was supported by the Chemical Sciences, Geosciences and Biosciences Division of Basic Energy Sciences, Office of Science, U.S. Department of Energy.

APPENDIX

In the molecular coordinate system, introduced in Sec. II, the scattering coordinate is taken to be the vector that joins the two nuclei, and the reduced mass for the system is that of the two nuclei. It has been argued [25] that the replacement of the nuclear reduced mass with the atomic reduced mass, in this coordinate system, accounts for some nonadiabatic corrections. In a rigorous treatment, the scattering coordinate for two asymptotically separated atoms is the vector that joins the two atom center of masses, and the reduced mass for the scattering coordinate is that of the two atoms. However, this particular Jacobi coordinate system is not well suited to the Born-Oppenheimer description that is appropriate in the molecular region. In this appendix, we provide an alternative description, in which we use the molecular coordinate system, but by a unitary transformation of the Hamiltonian, we arrive at a description in which the correct asymptotic Hamiltonian, where the system reduced mass is that of the two atoms, is manifest.

We define the unitary transformation

$$U_i \equiv \exp[-im/(m+M)\mathbf{P}_i\cdot\mathbf{x}_i]\exp(i\mathbf{p}_i\cdot\mathbf{R}_i), \tag{A1}$$

which has the following properties,

$$\begin{aligned} U_i\mathbf{R}_iU_i^\dagger &= \mathbf{R}_i - \frac{m}{M+m}\mathbf{x}_i, \\ U_i\mathbf{x}_iU_i^\dagger &= \mathbf{R}_i + \frac{M}{M+m}\mathbf{x}_i, \\ U_i\mathbf{P}_iU_i^\dagger &= \frac{M}{M+m}\mathbf{P}_i - \mathbf{p}_i, \\ U_i\mathbf{p}_iU_i^\dagger &= \mathbf{p}_i + \frac{m}{m+M}\mathbf{P}_i. \end{aligned} \tag{A2}$$

It follows that

$$\begin{aligned} H' \equiv U_1U_2HU_1^\dagger U_2^\dagger &= \frac{1}{2(M+m)}\mathbf{P}_1^2 + \frac{1}{2(M+m)}\mathbf{P}_2^2 + \frac{1}{2\mu_e}\mathbf{p}_1^2 \\ &+ \frac{1}{2\mu_e}\mathbf{p}_2^2 + V_{Ne}(\mathbf{x}_1) + V_{Ne}(\mathbf{x}_2) + V', \\ V' \equiv U_1U_2[V_{NN}(|\mathbf{R}_2-\mathbf{R}_1|) &+ V_{Ne}(|\mathbf{R}_2-\mathbf{x}_1|) \\ &+ V_{Ne}(|\mathbf{R}_1-\mathbf{x}_2|) + V_{ee}(|\mathbf{x}_1-\mathbf{x}_2|)]U_1^\dagger U_2^\dagger. \end{aligned} \tag{A3}$$

In Eq. (A3), $\mu_e \equiv m\,M/(m+M)$ is the reduced mass of the bound electron on the proton, and the subscripts NN, Ne, and ee denote nuclear-nuclear, nuclear-electron, and electron-electron electrostatic interactions terms, respectively. We simplify the expression for V' so that

$$\begin{aligned} V' = W_1W_2[V_{NN}(|\mathbf{R}_1-\mathbf{R}_2|) + V_{Ne}(|\mathbf{x}_2+\mathbf{R}_2-\mathbf{R}_1|) + V_{Ne}(|\mathbf{x}_1 \\ -\mathbf{R}_2+\mathbf{R}_1|) + V_{ee}(|\mathbf{x}_1-\mathbf{x}_2+\mathbf{R}_1-\mathbf{R}_2|)]W_1^\dagger W_2^\dagger \end{aligned} \tag{A4}$$

and

$$W_i \equiv \exp[-im/(m+M)\mathbf{P}_i\cdot\mathbf{x}_i]. \tag{A5}$$

We introduce the center of mass (c.m.) $\mathbf{R}_{c.m.}$ and relative position $\mathbf{R}$ vectors, along with the corresponding conjugate momenta $\mathbf{P}_{c.m.}$, $\mathbf{P}$. Thus,

$$\mathbf{R} = \mathbf{R}_2 - \mathbf{R}_1,$$

$$\mathbf{R}_{c.m.}=\tfrac{1}{2}(\mathbf{R}_1+\mathbf{R}_2),$$

$$\mathbf{P}_2=\mathbf{P}+\frac{\mathbf{P}_{c.m.}}{2}$$

$$\mathbf{P}_1=-\mathbf{P}+\frac{\mathbf{P}_{c.m.}}{2}. \tag{A6}$$

We then have

$$H'=H_0'+V', \tag{A7}$$

where

$$H_0'=\frac{1}{4(M+m)}\mathbf{P}_{c.m.}^2+\frac{1}{2\mu_H}\mathbf{P}^2+\frac{1}{2\mu_e}\mathbf{p}_1^2 + \frac{1}{2\mu_e}\mathbf{p}_2^2+V_{Ne}(\mathbf{x}_1)+V_{Ne}(\mathbf{x}_2) \tag{A8}$$

and $\mu_H\equiv(M+m)/2$ is the reduced mass for the pair of hydrogen atoms. Also,

$$V'=W[V_{Ne}(|\mathbf{x}_2+\mathbf{R}|)+V_{Ne}(|\mathbf{x}_1-\mathbf{R}|) + V_{ee}(|\mathbf{x}_1-\mathbf{x}_2-\mathbf{R}|)+V_{NN}(|\mathbf{R}|)]W^\dagger, \tag{A9}$$

where

$$W\equiv\exp[-im/(m+M)[\mathbf{P}\cdot(\mathbf{x}_2-\mathbf{x}_1)]. \tag{A10}$$

In deriving Eqs. (A7)–(A9), we made use of the fact that $\mathbf{P}_{c.m.}$ commutes with V'.

Consider the electronic Hamiltonian

$$h_{ad}\equiv\frac{1}{2\mu_e}\mathbf{p}_1^2+\frac{1}{2\mu_e}\mathbf{p}_2^2+V_{Ne}(\mathbf{x}_1)+V_{Ne}(\mathbf{x}_2) + W[V_{Ne}(|\mathbf{x}_2+\mathbf{R}|)+V_{Ne}(|\mathbf{x}_1-\mathbf{R}|) + V_{ee}(|\mathbf{x}_1-\mathbf{x}_2-\mathbf{R}|)+V_{NN}(|\mathbf{R}|)]W^\dagger, \tag{A11}$$

which can be rewritten as

$$h_{ad}=\exp(i[\mathbf{p}_2-\mathbf{p}_1]\cdot\mathbf{R}/2)h_{ad}'\exp(-i[\mathbf{p}_2-\mathbf{p}_1]\cdot\mathbf{R}/2), \tag{A12}$$

where

$$h_{ad}'=\frac{1}{2\mu_e}\mathbf{p}_1^2+\frac{1}{2\mu_e}\mathbf{p}_2^2+V_{Ne}(|\mathbf{x}_1+\mathbf{R}/2|)+V_{Ne}(|\mathbf{x}_2-\mathbf{R}/2|) + \mathcal{W}[V_{Ne}(|\mathbf{x}_1-\mathbf{R}/2|)+V_{Ne}(|\mathbf{x}_2+\mathbf{R}/2|) + V_{ee}(|\mathbf{x}_2-\mathbf{x}_1|)+V_{NN}(|\mathbf{R}|)]\mathcal{W}^\dagger \tag{A13}$$

and

$$\mathcal{W}\equiv\exp(-i\mathbf{p}_\xi\cdot\mathbf{R})\exp[-im/(m+M)\mathbf{P}\cdot\xi]\exp(i\mathbf{p}_\xi\cdot\mathbf{R}) =\exp[-im/(m+M)(\mathbf{P}+\mathbf{p}_\xi)\cdot(\xi-\mathbf{R})], \tag{A14}$$

where we introduced the symmetric coordinates

$$\xi\equiv\mathbf{x}_2-\mathbf{x}_1, \quad \mathbf{p}_\xi\equiv(\mathbf{p}_2-\mathbf{p}_1)/2. \tag{A15}$$

If we are allowed, in the limit $m/M\to 0$, to replace $\mathcal{W}$ with the identity operator we recognize that h_{ad}' is similar to the Born-Oppenheimer or adiabatic Hamiltonian discussed in Sec. II. It differs from H_{AD} given in Eq. (4), in that the mass of the electron is replaced by reduced mass of the electron in the hydrogen atom, and mass polarization terms are not present.

Using H' given in Eq. (A7), the adiabatic Hamiltonian, h_{ad}' in Eq. (A13), setting $\mathcal{W}$ equal to the unity operator, and repeating the procedure outlined in Sec. II, we obtain scattering equations (18), where the bare nuclear reduced mass is replaced by the reduced mass of the hydrogen atoms. In this picture, the lowest order potentials are, again, the BO potentials, but the adiabatic corrections differ from those given in Sec. II. A similar result is obtained if we replace $\mathbf{x}_i$ and $\mathbf{p}_i$ appearing in Eq. (A1) with terms in which the index i is replaced by index j, so that when $i=1$, $j=2$, and when $i=2$, $j=1$.

[1] E.M. Purcell and G.B. Field, Astrophys. J. **124**, 542 (1956).
[2] A. Dalgarno and M.H. Rudge, Astrophys. J. **140**, 800 (1964).
[3] A. Dalgarno and R.A. McCray, Ann. Rev. Astron. Astrphys. **10**, 375 (1972).
[4] D.R. Bates, Proc. Phys. Soc. B **64**, 805 (1951).
[5] A. Dalgarno and R.J.W. Henry, Proc. Phys. Soc. **83**, 157 (1964).
[6] R. Sharma, B. Zygelman, F. von Esse, and A. Dalgarno, Geophys. Res. Lett. **21**, 1731 (1994).
[7] T.G. Walker and W. Happer, Rev. Mod. Phys. **69**, 629 (1997).
[8] T. Chupp and S. Swanson, Adv. At., Mol., Opt. Phys. **45**, 42 (2001).
[9] P.L. Bender, Phys. Rev. **132**, 2154 (1963).
[10] L.C. Balling, R.J. Hanson, and F.M. Pipkin, Phys. Rev. **133**, A607 (1964).
[11] S.B. Crampton, Phys. Rev. **158**, 57 (1967).
[12] S.B. Crampton, J.A. Duvivier, G.S. Read, and E.R. Williams, Phys. Rev. A **5**, 1752 (1972).
[13] A.C. Allison, Phys. Rev. A **5**, 2695 (1972).
[14] A. Dalgarno, Proc. R. Soc. London, Ser. A **262**, 132 (1961).
[15] J.P. Wittke and R.H. Dicke, Phys. Rev. **103**, 620 (1956).
[16] A. Dalgarno and M.R.H. Rudge, Proc. R. Soc. London, Ser. A **286**, 519 (1965).
[17] A.C. Allison and A. Dalgarno, Astrophys. J. **158**, 423 (1969).
[18] F.J. Smith, Planet. Space Sci. **14**, 929 (1966).
[19] A.J. Berlinsky and B. Shizgal, Can. J. Phys. **58**, 881 (1980).
[20] H.R. Cole and R.E. Olson, Phys. Rev. A **31**, 2137 (1985).
[21] N. Koyama and J.C. Baird, J. Phys. Soc. Jpn. **55**, 801 (1986).
[22] M.J. Jamieson, A. Dalgarno, and J.N. Yukich, Phys. Rev. A **46**, 6956 (1992).
[23] S.B. Crampton, Ph.D. thesis, Harvard University, 1964 (unpublished).
[24] S.B. Crampton and H.T.M. Wang, Phys. Rev. A **12**, 1305 (1975).

[25] B.J. Verhaar, J.M.V.A. Koelman, H.T.C. Stoof, O.J. Lueton, and S.B. Crampton, Phys. Rev. A **35**, 3825 (1987).
[26] J.M.V.A. Koelman, S.B. Crampton, H.T.C. Stoof, O.J. Luiton, and B.J. Verhaar, Phys. Rev. A **38**, 3535 (1988).
[27] S.J.J.M.F. Kokkelmans and B.J. Verhaar, Phys. Rev. A **56**, 4038 (1997).
[28] M.E. Hayden, M.D. Hurlimann, and W.N. Hardy, IEEE Trans. Instrum. Meas. **42**, 314 (1993).
[29] M.E. Hayden and W.N. Hardy, J. Low Temp. Phys. **99**, 787 (1995).
[30] M.E. Hayden, M.D. Hurlimann, and W.N. Hardy, Phys. Rev. A **53**, 1589 (1996).
[31] M.E. Hayden and W.N. Hardy, Phys. Rev. Lett. **76**, 2041 (1996).
[32] R.L. Walsworth, I.F. Silvera, E.M. Mattison, and R.F.C. Vessot, Phys. Rev. A **46**, 2495 (1992).
[33] W. Kolos and J. Rychlewski, J. Chem. Phys. **98**, 3960 (1993).
[34] W. Kolos, J. Chem. Phys. **101**, 1330 (1994).
[35] L. Wolniewicz, J. Chem. Phys. **99**, 1851 (1993).
[36] We include the mass polarization term in our definition of the adiabatic Hamiltonian.
[37] B. Zygelman, A. Dalgarno, and R.D. Sharma, Phys. Rev. A **49**, 2587 (1994).
[38] A. Dalgarno and R. McCarroll, Proc. R. Soc. London, Ser. A **256**, 383 (1956).
[39] D.R. Bates and R. McCarroll, Proc. R. Soc. London, Ser. A **247**, 158 (1958).
[40] H.A. Bethe and E.E. Salpeter, *Quantum Mechanics of the One- and Two-Electron Atoms* (Academic Press, New York, 1957).
[41] C.H. Townes and A.L. Schawlow, *Microwave Spectroscopy* (McGraw-Hill, Tokyo, 1955), p. 196.
[42] B.R. Johnson, J. Comput. Phys. **13**, 445 (1973).
[43] B.R. Johnson, Phys. Rev. A **32**, 1241 (1985).
[44] R.F.C. Vessot, M.W. Levine, E.M. Mattison, E.L. Blomberg, T.E. Hoffmann, G.U. Nystrom, and B.F. Farrel, Phys. Rev. Lett. **45**, 2081 (1980).
[45] S.B. Crampton, W.D. Phillips, and D. Kleppner, Bull. Am. Phys. Soc. **23**, 86 (1978).
[46] M. Desaintfuscien and C. Audoin, Phys. Rev. A **13**, 2070 (1976).
[47] M. Jamieson and B. Zygelman, Phys. Rev. A **64**, 032703 (2001).